Ocean Engineering 175 (2019) 113–121

Contents lists available at ScienceDirect

Ocean Engineering

journal homepage: www.elsevier.com/locate/oceaneng

Modeling the large runup along a narrow segment of the Kaikoura coast, New Zealand following the November 2016 tsunami from a potential landslide

Mohammad Heidarzadeh[a,*], David R. Tappin[b,c], Takeo Ishibe[d]

[a] Department of Civil & Environmental Engineering, Brunel University London, Uxbridge, UB8 3PH, UK
[b] British Geological Survey, Keyworth, Nottingham, NG12 5GG, UK
[c] UCL Hazard Centre, University College London, WC1E 6BT, UK
[d] Association for the Development of Earthquake Prediction, Tokyo, 101-0064, Japan

ARTICLE INFO

Keywords:
New Zealand
2016 Kaikoura earthquake
Submarine landslide
Tsunami
Numerical simulations
Dual tsunami source

ABSTRACT

The 2016 *Mw* 7.8 Kaikoura earthquake and consequent tsunami have been controversial because of uncertainty over whether and where the plate interface ruptured and the incapability of the proposed source models to reproduce the near-field runup of 7 m. Existing models identify a wide range of locations for the interface rupture, from on land to offshore, and fail to reproduce runup of 7 m near Kaikoura. To generate the large tsunami peak in Kaikoura tide gauge record and the observed runup height, offshore seafloor movement is necessary, but the offshore extension of the plate-interface rupture and its type, either seismic rupture or a landslide, is uncertain. Here, we propose a submarine landslide in addition to the earthquake source, with the landslide delayed 10–20 min after the earthquake rupture. The landslide volume is 4.5–5.2 km^3, located within 173.7–174.3°E (longitude) and 42.6–42.15°S (latitude). Our proposed dual tsunami source successfully reproduces near-field tide gauge records as well as observed near-field runup height of 7 m. We showed that more accurate source models of earthquakes can be achieved by considering observed runup data through runup inversions in addition to waveform inversions.

1. Introduction and background

A few years after the November 2016 Kaikoura earthquake and tsunami (Fig. 1a), the debate about the source of the earthquake and the characteristics of the resulting tsunami continues. The Kaikoura earthquake, with moment magnitude (Mw) of 7.8, struck on the 13 November 2016 at 11:02:56 UTC (Fig. 1a, USGS: US Geological Survey). It generated a tsunami with maximum runups of up to 7 m (Lane et al., 2017; Power et al., 2017). A large concentrated coastal runup was observed along a narrow segment of the coast close to Kaikoura (Fig. 1c; latitude of 42.5°S). The mainshock's focal mechanism is complicated, with oblique thrust faulting, initiating strike-slip movement, followed by both strike-slip and thrust faulting (Duputel and Rivera, 2017; Hollinsworth et al., 2017). One commonality of the different proposed source mechanisms (Duputel and Rivera, 2017; Hollinsworth et al., 2017) is the occurrence of reverse faulting at the plate-interface. Major uncertainties, however, are whether the plate-interface ruptured or not; and if ruptured, whether the plate-interface rupture was offshore or on land. Some models confine the plate-interface rupture to on land, others extend it offshore, and some models lack any plate-interface rupture. Earthquake rupture location has major implications on seismic hazard in the region [e.g. Furlong and Herman, 2017], but also on tsunami generation.

Several source models have been proposed following the Kaikoura event, but none of them was able to reproduce the large concentrated runup of ~7 m observed in Kaikoura. Simulations from two state-of-the-art source models for the Kaikoura event generates up to 4 m of runup (pink and green lines, Fig. 1c) which is much smaller than observations (blue circles, Fig. 1c). The Kaikoura runup case reminds the challenge of the 1998 Papua New Guinea (PNG) tsunami whose observed concentrated runup of 15 m was only reproduced by a combined earthquake and a submarine landslide source (Okal, 1999; Tappin et al., 2001; Synolakis et al., 2002). The study by Okal and Synolakis (2004) revealed that unusually-large and concentrated runups are most likely the results of contribution of an additional co-seismic landslide source to the tsunami. Such combined earthquake-landslide sources are known as dual tsunami sources. Dual source earthquake and submarine landslide tsunamis are a poorly understood hazard, because there are too

* Corresponding author.
E-mail addresses: mohammad.heidarzadeh@brunel.ac.uk (M. Heidarzadeh), drta@bgs.ac.uk (D.R. Tappin), ishibe@erc.adep.or.jp (T. Ishibe).

https://doi.org/10.1016/j.oceaneng.2019.02.024
Received 13 September 2018; Received in revised form 9 December 2018; Accepted 3 February 2019
Available online 14 February 2019

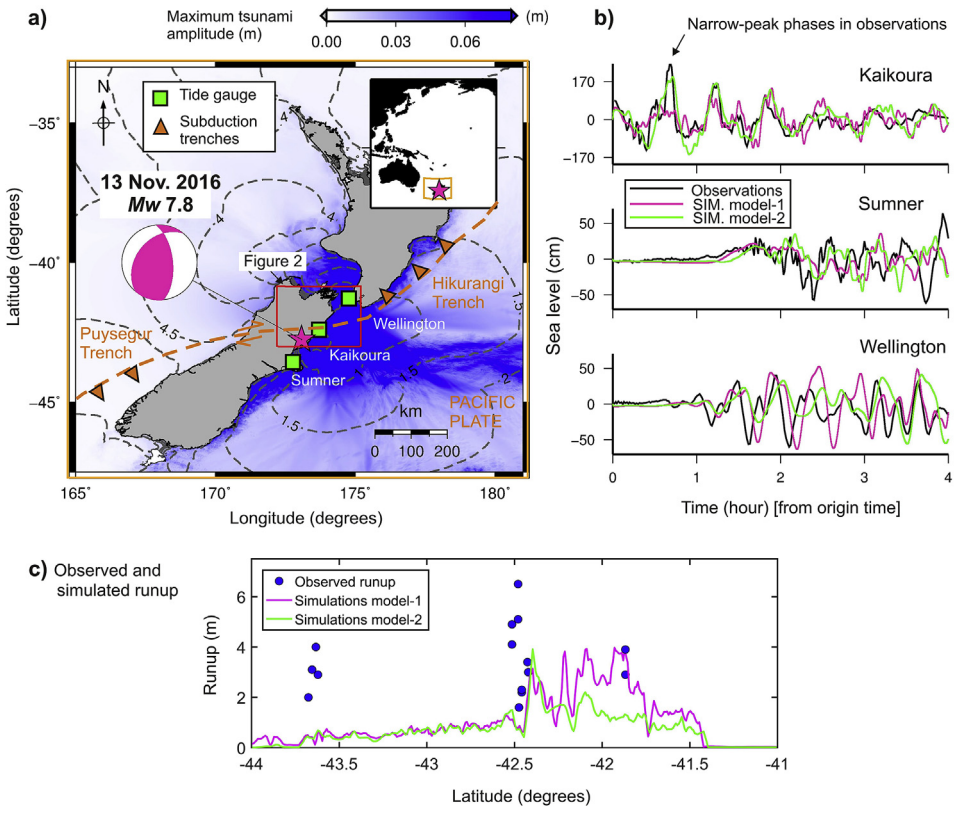

Fig. 1. a): Study area. Dashed contours are tsunami travel times in hour calculated using TTT program of Geoware (2011). The color map shows the distribution of maximum tsunami amplitude using the source model of Hamling et al. (2017). b): Observed (black) and simulated (pink and green) waveforms at three near-field tide gauge stations. Simulations are based on the source models by Hamling et al. (2017) (pink, model-1) and Gusman et al. (2018) (green, model-2). c): Observed and simulated runup heights from two source models (model-1 and model-2). *OBS* and *SIM* stand for *Observations* and *Simulations*, respectively. (For interpretation of the references to color in this figure legend, the reader is referred to the Web version of this article.)

few well-studied examples. The most notable dual events include: Messina (1908) (Billi et al., 2008; Fu et al., 2017), Makran (1945) (Heidarzadeh and Satake, 2017a), Alaska (1946) (Okal et al., 2002, 2003), Java (2006) (Fritz et al., 2007) and Japan (2011) (Tappin et al., 2014).

Here we review the source models for the 2016 Kaikoura tsunami. Based on the preliminary results of Heidarzadeh and Satake (2017b), rather than an offshore plate-interface rupture, we present supporting numerical models for an additional submarine landslide which is able to successfully reproduce the near-field observed runup of 7 m. The location of the submarine landslide source is determined based on the iterative numerical tsunami modeling of various scenarios of dual earthquake-landslide sources. The dual source model presented here for the 2016 Kaikoura tsunami is the only source model that reproduces both tide gauge records and the observed near-field runup heights.

2. Kaikoura tsunami source models

Co-seismic deformation of the Kaikoura earthquake includes rupture of at least 12 major faults (Hamling et al., 2017). The aftershocks are a mix of thrust and strike-slip faulting. Identification of the rupture location varies with the data sets and the methods used for analysis (Furlong and Herman, 2017). Hamling et al. (2017) (Fig. 2b), from geodetic and coastal uplift inversion, proposed two tectonic mechanisms: one with and one without slip on the plate-interface fault. Both slip models are located mainly on land where the plate-interface movement is also located. Neither reproduces the near-field tsunami observation at the Kaikoura tide gauge (pink lines, Fig. 1b) and the observed runup (pink lines, Fig. 1c). Bai et al. (2017), based on teleseismic inversion and forward tsunami simulations, proposed a three-segment, offset fault rupture, comprising two crustal and one plate-interface faults (Fig. 2c). These faults are located mainly on land, but with a plate-interface fault extended ~40 km offshore of Kaikoura. The model by Bai et al. (2017) successfully reproduced near-field tide gauge records, but the authors did not investigate if their source model is able

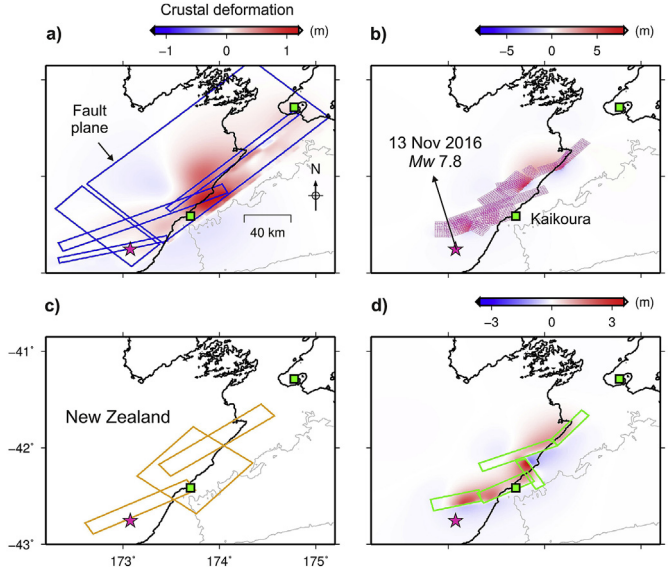

Fig. 2. a-d): Source models based on (a) USGS, (b) Hamling et al. (2017), (c) Bai et al. (2017), and (d) Gusman et al. (2018). Rectangles show fault planes while color maps are calculated crustal deformations generated by each source model. (For interpretation of the references to color in this figure legend, the reader is referred to the Web version of this article.)

to reproduce the near-field runup of 7 m. Heidarzadeh and Satake (2017b), based on short-period waves recorded at local tide gauges, proposed an alternative solution to the problem of the source location (Fig. S1). To explain the recorded tsunami, they suggested the addition (to the earthquake) of a submarine landslide. The possibility of a submarine landslide is supported by the near-field narrow peak tsunami recorded at the Kaikoura tide gauge (Fig. 1b). Support for the landslide hypothesis has been provided by Gusman et al. (2018). These authors,

Table 1
Parameters of all landslide scenarios considered in this study.

Landslide Scenario (LS)	Location (°E) (°S)	Length (km)	Width (km)	Thickness (m)	Volume (km^3)[a]	Water depth (m)	Travel distance (m)	Max. initial sea level depression (m)	Max. initial sea level elevation (m)
1	174.61 −42.085	10	10	150	4.47	2000	2000	−1.02	0.78
2	174.35 −42.20	10	10	150	4.47	1500	2000	−1.58	1.22
3	173.97 −42.3	10	10	175	5.22	1000	2000	−2.21	1.712
4	173.8 −42.415	10	10	150	4.47	1000	2000	−1.58	1.23
5	173.98 −42.511	10	10	175	5.22	1500	2000	−2.22	1.72
6	173.86 −42.713	10	10	175	5.22	1500	2000	−2.22	1.72
7	173.75 −43.0	10	10	150	4.47	1500	2000	−1.57	1.23
8	174.65 −42.72	10	10	150	4.47	2000	2000	−1.02	0.77
9	174.0 −42.3	10	10	150	4.47	500	2000	−3.49	2.71
10	174.0 −42.5	15	15	300	20.14	1500	2000	−2.94	2.23
11	173.7 −42.4	10	30	200	17.89	1000	2000	−2.67	2.43
12	173.6 −42.34	12	33	150	17.72	1000	2000	−0.19	1.10
13	173.6 −42.34	15	45	150	30.2	1000	2000	−0.31	0.85
14	173.6 −42.34	15	60	200	53.7	1000	2000	−0.65	1.52
15	173.6 −42.34	15	60	200	53.7	1000	2000	−1.23	1.53
16	173.69 −42.398	12	35	150	18.8	1000	2000	−1.20	1.10
17	173.837 −42.449	12	35	150	18.8	1000	2000	−1.42	1.10
18	173.8 −42.415	10	10	100	2.98	1000	2000	−0.64	0.495

[a] Calculated using equation 2 of Enet and Grilli (2007).

based on the inversion of the recorded tsunami waves, identified a tsunami-related sea surface disturbance (Fig. 2d). They speculated that the disturbance was from either an offshore plate-interface rupture or, alternatively, a submarine landslide. Although the model by Gusman et al. (2018) reproduces the Kaikoura tide gauge record (green lines, Fig. 1b), it cannot reproduce the near-field runup of 7 m (green lines, Fig. 1c).

Although some source models successfully reproduced the Kaikoura tide gauge record (Gusman et al., 2018; Bai et al., 2017), none of them reproduces the near-field runup of 7 m (Fig. 1c). This has been the major challenge associated with the 2016 Kaikoura tsunami. Spectral analysis of tide gauge data (Heidarzadeh and Satake, 2017b) showed a dual-peak spectrum for the tsunami (Fig. S1), which is unusual for a purely-tectonic event, and is more suggestive of a confined secondary mechanism, such as a submarine landslide. A submarine landslide mechanism is also supported by the numerical simulations of Heidarzadeh and Satake (2017b) which, based on the purely earthquake source model, revealed an energy deficit compared to the tide gauge observations for the short-period band of < 7 min. In this context, to explain the observed near-field runup of 7 m, we examine the possibility of the contribution of a submarine landslide to the 2016 Kaikoura tsunami.

3. Data and methods

We used three near-field tsunami observations from tide gauges at Kaikoura, Sumner and Wellington (Fig. 1) provided by the GNS Science New Zealand and Land Information New Zealand. We applied Welch algorithm of Mathworks (2017) for Fourier analysis following the procedure described in Rabinovich (1997). Numerical modeling of tsunami was performed using combined earthquake-landslide sources. The earthquake source model was based on that of Hamling et al. (2017) with interplate rupture; although both crustal and interplate models of Hamling et al. (2017) yield similar tsunami waves (Heidarzadeh and Satake, 2017b). This model contains slips on 19 faults with varying strike, dip and rake angles and having a maximum slip of 24.1 m for the strike-slip component and slip of up to 10 m for the reverse component. Then, hypothetical landslide sources were added. The analytical solution by Okada (1985) was used for constructing initial seafloor deformation for the earthquake source (using input parameters of Hamling et al., 2017), while the semi-empirical equations of Watts et al. (2003, 2005) were used to construct the initial sea surface deformation due to the landslide. The numerical model of Satake (1995) was used for tsunami simulation, with a time step of 1.0 s on the 30 arc-sec bathymetry grid of General Bathymetric Charts of the Oceans (GEBCO, Weatherall et al., 2015). This numerical model solves nonlinear shallow water equation. Inundation modeling is not included because high-resolution bathymetry/topography data has not been available for our study. We record wave oscillation on a coastal vertical wall which gives an approximation of wave runup (Tinti et al., 2006; Satake et al., 2013). Although our 30 arc-sec bathymetry grid is not capable of resolving small-scale coastal features such as ports and bays, our approach results in reasonable approximation of the overall runup behavior as shown by Tinti et al. (2006) and Heidarzadeh et al. (2009). To measure the quality of fit between observations and simulations, we used the Normalized Root Mean Square (NRMS) misfit equation of

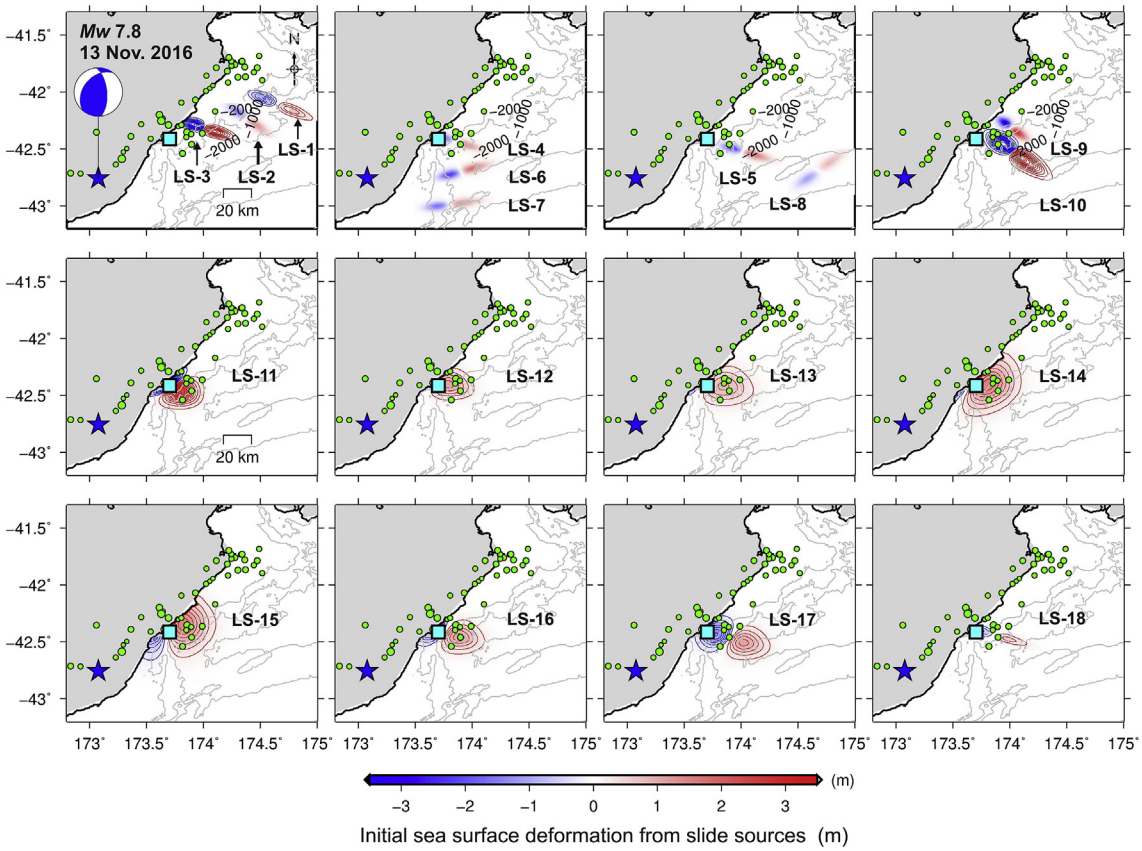

Fig. 3. The initial sea surface deformation due to landslide scenarios 1 to 18 (LS-1 to LS-18). Star shows the location of the November 2016 epicenter. Detailed information about each of these landslide sources are given in Table 1. Some of the landslide scenarios are shown as contours in order to be clearly identifiable when the scenarios overlap each other. The blue and red contours represent depression and elevation, respectively. Contour intervals are 0.1 m. (For interpretation of the references to color in this figure legend, the reader is referred to the Web version of this article.)

Heidarzadeh et al. (2016a). The comparison was made for the first few tsunami waves (first 30–60 min).

The semi-empirical equations of Watts et al. (2003, 2005), which estimate the 3D sea surface at the end of landslide motion, has been successfully applied by several authors for landslide-generated waves (Synolakis et al., 2002; Satake and Tanioka, 2003; Okal and Synolakis, 2004; Tappin et al., 2008; Heidarzadeh et al., 2014; Heidarzadeh and Satake, 2015a, 2017a). Landslide parameters were: length, 10–15 km; width, 10–60 km; water depth at the center of slide, 500–2000 m, thickness: 100–300 m; bulk density: 2150 kg m^{-3} (Watts et al., 2003) and travel distance: 2000 m (Table 1). We note that the travel distance can vary at different locations due to different slop angles, but we have fixed it here to decrease the number of landslide scenarios. The shape of the initial mass is considered to be Gasussian (Watts et al., 2005; Enet and Grilli, 2007). Landslides were aligned approximately normal to the downslope direction of travel. Simultaneous dipoles (e.g. Synolakis et al., 2002) were used. In total, 18 landslide scenarios (LS) were tested located all over onshore and offshore Kaikoura (Fig. 3). Among various landslide parameters, our LSs (Table 1) well constrain length, width, thickness and location (water depth) of a potential landslide. The criteria for choosing the landslide locations and sizes were to cover the entire Kaikoura Canyon and to generate waves with periods and amplitudes similar to those of the observations, respectively. Slope angles were in the range of 4-10%; a mean slope angle of 8% was considered for all scenarios. As per Watts et al. (2005), the added mass and drag coefficients are assumed to be one in this study.

The landslide and earthquake sources of the tsunami were simulated separately using linear models; then, these models were superimposed to form the simulation from the combined earthquake-landslide tsunami source. Heidarzadeh et al. (2016a) showed that linear and nonlinear tsunami simulations produce the same results at the coastal tide gauges, before inundation stage where nonlinearity is small. As the dimensions of our proposed landslide mechanism (length and width of 10 km and sea surface projection of ~25 km) are several times larger than the water depth (~1000 m) in this study, application of the shallow water model is justified (e.g. Synolakis et al., 2002; Synolakis and Kanoglu, 2015). This method has successfully reproduced the actual tsunami observations from the 1998 Papua New Guinea (PNG) dual earthquake-landslide tsunami by Heidarzadeh and Satake (2015a). Tsunami modeling is not sensitive to the timing of the earthquake rupture because tsunamis travel approximately 20–100 times slower than seismic waves (Heidarzadeh et al., 2016b).

Dispersion of landslide-generated waves has been reported in previous studies (Ren et al., 2015). Glimsdal et al. (2013) presented the parameter τ which determines the degree of wave dispersion:

$$\tau = \frac{6h^2 L}{\lambda^3} \quad (1)$$

in which h is water depth at the source region, λ is source length (or wavelength) and L is the distance from source region to the shore. According to Glimsdal et al. (2013), dispersion effect is negligible for $\tau < 0.01$ and it becomes significant for $\tau > 0.1$. For our landslide scenarios 3 and 4, we have: $\lambda = 10\ km$ (Table 1), $L = 0 - 10\ km$ (Fig. 3) and $h = 0 - 1000\ m$ (Fig. 3). Therefore, $\tau \sim 0.005$ (by assuming $L = 5\ km$ and $h = 500\ m$) which indicates dispersion effects can be ignored in our study justifying application of nonlinear shallow water equations.

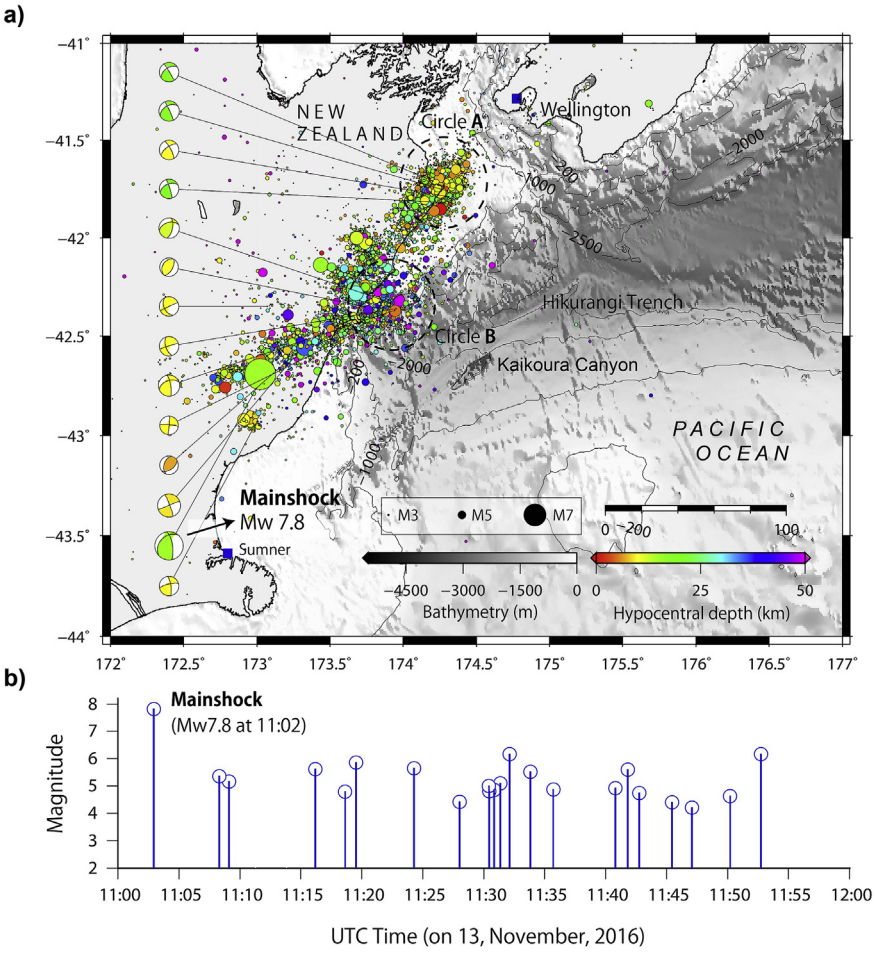

Fig. 4. a): Bathymetry of Kaikoura Canyon along with the one-month aftershocks (circles). The data are from the Geological hazard information for New Zealand (GeoNet) and the Global Centroid-Moment-Tensor (CMT) Project. Two dashed circles show two regions of major offshore aftershock activities. b): Magnitude-time plot of the aftershocks during the first 1 h following the mainshock.

4. Potential landslide locations and triggering mechanisms offshore Kaikoura

The pre-earthquake marine geology of the Kaikoura Canyon is well described (Lewis and Barnes, 1999; Walters et al., 2006; Mountjoy et al., 2018) and several seabed features support a significant potential for submarine landslides. The Canyon cuts across the shelf, almost reaching the coast of Kaikoura (Fig. 4a and S2), so that water depths close offshore increase rapidly seaward, with steep gradients of approximately 45° (Fig. S2). Around 5 km offshore, water depths reach 1000 m (Fig. 4a and S2). Here, a large deposit of unstable or slumped seabed material located at a deeply incised canyon head region was identified by Lewis and Barnes (1999). Walters et al. (2006) studied tsunamigenic landslides within the Kaikoura Canyon, and their numerical modeling of landslide scenarios at shallow water depths (less than 100 m) gave an initial wave of up to 13 m (Walters et al., 2006). After the 2016 Kaikoura earthquake, marine surveys in the Kaikoura Canyon head, identified major landslides triggered by the 2016 earthquake (Massey et al., 2018; Mountjoy et al., 2018). Comparison of the before and after bathymetry in the Canyon reveals that the total net erosion volume of sediment removed from the canyon floor was 0.94 km^3, a figure which does not include sediment shed from the canyon walls. Farther north off of North Island, (north of latitude 42°S), post-earthquake seismic data reveals vertical seabed fault movement, and seabed coring sampled turbidity currents from submarine landslides (Tangaroa TAN1613 Voyage Report: https://www.niwa.co.nz/static/web/Vessels/TAN1613-Voyage-Report_Hikurangi-Subduction-Zone-web.pdf).

There are two regions of intense aftershock activity offshore of the Kaikoura earthquake epicenter (Fig. 4a; dashed Circles A and B). The northern circle is where Hamling et al. (2017) identified the offshore fault rupture. The second cluster of offshore aftershocks is located near Kaikoura, in the vicinity of the Kaikoura Canyon (Circle B; Fig. 4a). The intense seismic activity offshore of Kaikoura has the potential to trigger submarine landslide as it is within the Kaikoura Canyon. Magnitude-time plot (Fig. 4b) shows that several moderate-size earthquakes (Mw 5–6) occurred within the first hour following the main shock. The seismic data from the local network (e.g. GeoNet) may help to identify the seismic signature of potential submarine landslides (e.g. Synolakis et al., 2002).

5. Results of numerical modeling

Simulation results of 18 LSs are presented in Fig. 5 and S3. The LSs located to the northeast of Kaikoura in shallower water depths of ~1000 m (LS-3 and LS-4 in Figs. 5 and 6 and S3) result in waves with amplitudes and periods comparable to those recorded at tide gauges. The other landslide scenarios at water depths of ~1500–2000 m produce very short-period waves (e.g. LS 1–2 and 5–8 in Fig. 5 and S3). Several authors have shown that tsunami periods are directly correlated to the water depth of the source (Watts et al., 2003; Fritz et al., 2004; Geist et al., 2009; Satake et al., 2013): the shallower the water depth, the longer the period of the generated waves.

The earthquake-generated waveforms (Fig. 6a) were superimposed

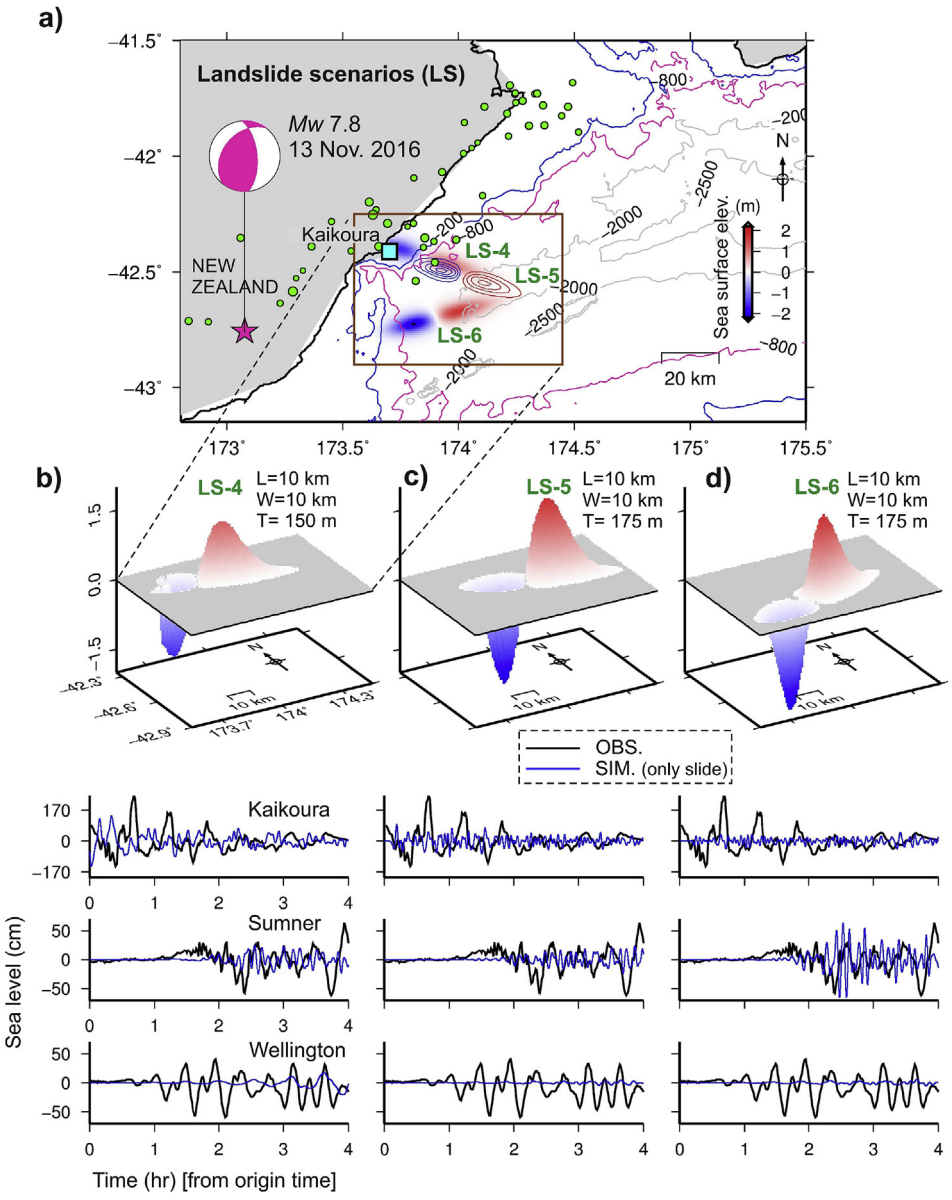

Fig. 5. Results of simulations of hypothetical landslide scenarios for three of the landslide scenarios. a): Location of the three landslide scenarios and one-day USGS aftershocks (green circles). Some of the landslide scenarios are shown as contours in order to be clearly identifiable when the scenarios overlap each other. b-d): From top to bottom: 3D projection of the landslide source; observed and simulated waveforms from the purely-landslide source. L, W and T represent length, width and thickness of the landslide, respectively. *OBS* and *SIM* stand for *Observations* and *Simulations*, respectively. (For interpretation of the references to color in this figure legend, the reader is referred to the Web version of this article.)

on those generated by the landslides (Fig. 6b) to produce tsunami simulations from a combined (dual) source (Fig. 6c). To reproduce the short-period, large peak tsunami wave at Kaikoura for LS-3 and LS-4 (Figs. 1b and 6c), we found that the landslide required triggering ~10 and ~20 min after the earthquake, respectively, based on the timing of the narrow peak in the Kaikoura record. The wavelet analysis by Heidarzadeh and Satake (2017b) also revealed an approximately 20 min delay in the arrival of the short-period waves of the 2016 Kaikoura tsunami. A delay in landslide triggering has been found at other dual tsunami source events, such as the well documented 13–15 min delay for the landslide part of the 1998 Papua New Guinea tsunami (Okal, 1999; Tappin et al., 2001; Synolakis et al., 2002; Heidarzadeh and Satake, 2015a). The occurrence of several medium-size magnitude aftershocks (*M* 5–6) within 30 min of the 2016 Kaikoura main shock (Fig. 4b) supports these as a potential triggering mechanism. The plot of NRMS misfits for various landslide scenarios (Fig. 6d) yields minimum misfits of 1.01 and 1.03 for LS-3 and LS-4, respectively. The NRMS misfits from our final landslide source scenarios (LS-3 and LS-4 in Fig. 6c) are close to that from the inversion-based tsunami source model of Gusman et al. (2018) (green line in Fig. 6c and d).

From our numerical simulations of the various dual-source scenarios, we consider the most likely location of the submarine landslide source is at a water depth of ~1000 m on the slope of the Kaikoura Canyon, within the area of intense aftershock-activity, offshore Kaikoura (LS-3 and LS-4 in Fig. 6b and Circle B in Fig. 4a). Based on the numerical results, we identify the zone shown by Box A in Fig. 6b (longitude: 173.7–174.3°E; latitude: 42.6–42.15°S) as the most likely landslide zone. The dimensions of this landslide source are length, 10 km; width, 10 km; and thickness, 150–175 m resulting in a slide volume of 4.5–5.2 km^3 (Fig. 6c and Table 1). The landslide-generated waveforms (Fig. 5b) show typical behavior generally expected from confined landslide sources: first, they are large in the near field (i.e. large amplitudes at Kaikoura) and rapidly lose amplitude farther from the source region (i.e. small amplitudes in Sumner and Wellington); and second, the landslide waveforms contain few large peaks which disappear rapidly as seen in the simulated waveforms at Kaikoura (Fig. 5b).

Comparison of observed and simulated runup heights (Fig. 7) supports that a narrow-focused landslide source can successfully reproduce the peak tsunami runup of 7 m observed in Kaikoura. The two purely-tectonic sources of Hamling et al. (2017) and Gusman et al. (2018) were unable to reproduce such large runup heights in Kaiokoura (Fig. 1c).

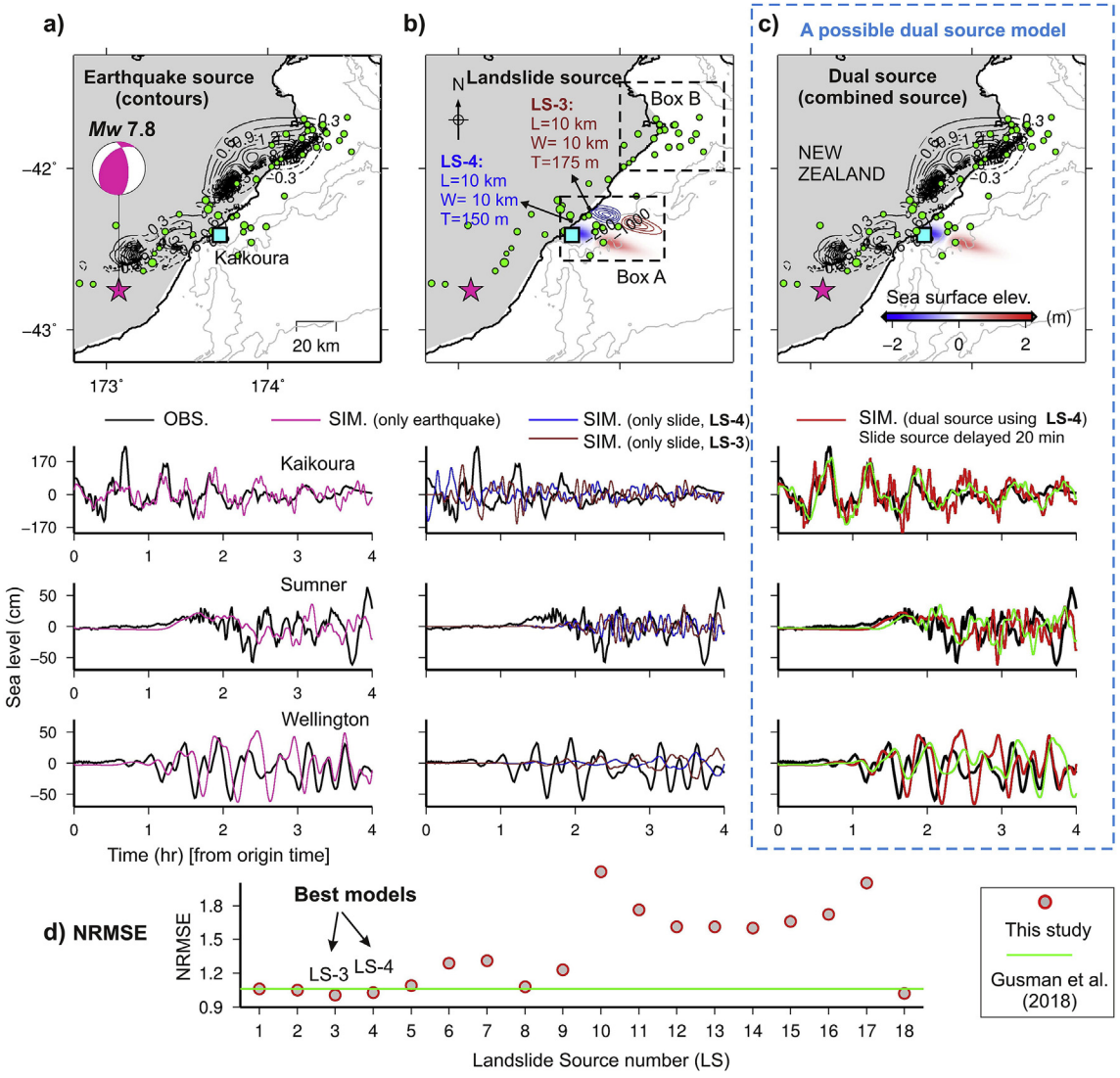

Fig. 6. Simulations of a possible combined earthquake-landslide source model. a): Purely-earthquake source; b): Purely-landslide sources; c): A possible combined earthquake-landslide source. From top to bottom: location of the source and one-day USGS aftershocks; and observed and simulated waveforms. d) Normalized Root Mean Square (NRMS) misfits for different LSs. *OBS* and *SIM* stand for *Observations* and *Simulations*, respectively.

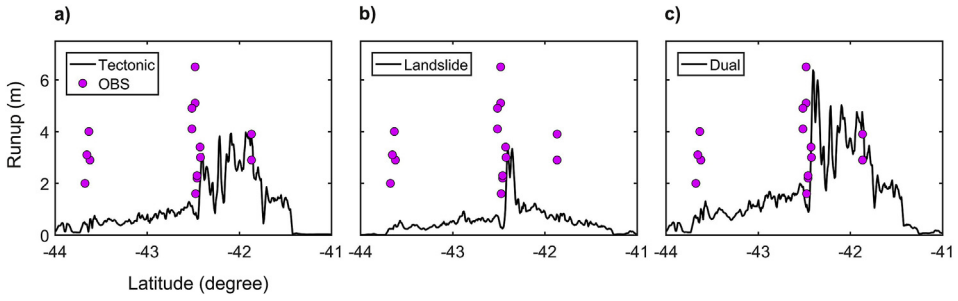

Fig. 7. Comparison of simulated (solid line) and observed runup heights (pink circles; based on Power et al., 2017) for (a) the purely-tectonic source, (b) the purely-landslide source, and (c) the combined dual (earthquake-landslide) source. *OBS* and *SIM* stand for *Observations* and *Simulations*, respectively. (For interpretation of the references to color in this figure legend, the reader is referred to the Web version of this article.)

Fourier analyses of the various waveforms (i.e. observations, purely-tectonic, purely-landslide and combined sources) are shown in Fig. 8. As expected, landslide-generated waves mainly contribute to spectral energy at periods < 7 min due to their confined source dimensions. The spectral energy for the combined source is noticeably increased at periods < 7 min while it is almost same as that of the purely-tectonic source for periods > 7 min (Fig. 8). Such effects are not seen at the Wellington station as it is located within a semi-enclosed bay where bathymetric features mostly filter the landslide-generated short-period waves before reaching there (Heidarzadeh and Satake, 2017b).

6. Discussions

Although the occurrence of a plate-interface rupture is likely during the Kaikoura event (Duputel and Rivera, 2017; Hollinsworth et al., 2017), the state-of-the-art knowledge on earthquake source process does not allow such a plate-interface rupture to be precisely located. The plate-interface rupture components of Hamling et al. (2017) and

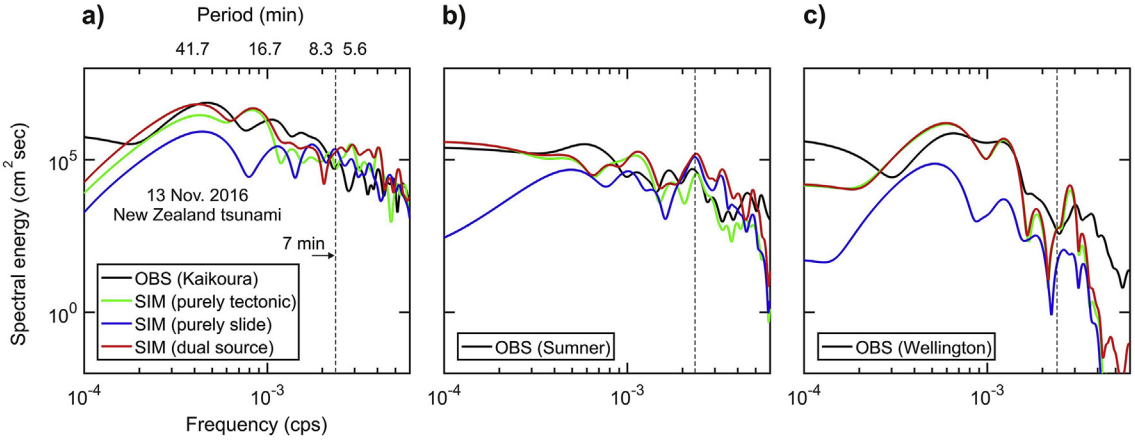

Fig. 8. Fourier analyses for the simulated and observed waveforms from the purely-tectonic, purely-landslide and the combined (dual) sources. The dashed line at the period of 7 min is roughly the cut-off period for landslide-generated waves. *OBS* and *SIM* stand for *Observations* and *Simulations*, respectively.

Bai et al. (2017) are distanced ~ 50 km, with the former located fully on land while the latter is partly offshore. Several authors (e.g. Heidarzadeh et al., 2016b, 2017a, b; Gusman et al., 2015, Lay et al., 2014) have shown that seismic inversions are sensitive to the choice of rupture velocity (*Vr*). Because of this, rupture location can vary up to tens of kilometers.

In addition to large and concentrated runup height of 7 m in Kaikoura, another patch of concentrated measured runup of ~4 m is observed around the latitude of 43.66 °S while simulations result in a runup value of ~0.5 m (Fig. 7, black line). It is possible that another submarine landslide has contributed to the elevated runup here. As intensive landslide activities were reported following the Kaikoura earthquake with thousands of landslides mapped in post-event field surveys, such a scenario looks possible. We note that based on the modeling results from 18 landslide scenarios (Fig. 3, Fig. S3), it is clear that the landslide scenario proposed offshore Kaikoura (LS-3, Fig. 6c) cannot be extended to cover the latitude of 43.66 °S because, if we expand it, the resulting waveforms will not match the observed waveforms (Fig. S3). In other words, to reproduce the runup of 4 m around the latitude of 43.66 °S, another isolated landslide scenario is required with dimensions potentially smaller than our LS-3. Therefore, two isolated landslide sources will be required to match the observed runup distribution. An example for occurrences of several isolated submarine landslides following an earthquake, which contributed to elevated runup heights in several locations, is the 1956 Amorgos (Greece) event (Okal et al., 2009). The elevated runup heights at several locations following the 1956 tsunami were explained by addition of several isolated landslide sources to the tectonic source of the earthquake by Okal et al. (2009).

The novelty of our dual model over published source model (e.g. Gusman et al., 2018; Hamling et al., 2017) is that it reproduces the observed runup data whereas other source models failed. The other studies are based on the common practice and well-established method of seismic/tsunami waveform inversions which matches the observed point waveforms using a least-square or similar optimization techniques. This technique is very strong, but it needs a suitable number of observation points to accurately map the earthquake source characteristics. Especially, this method may not result in accurate enough source models if a landslide is involved because landslide-generated water waves travel short distances and thus a scattered observation network may miss them; and landsides produce almost trivial seismic waves and hence there will be almost no trace of them on the seismic observation network. In fact, this study highlights the importance of considering observed runup data for earthquake source studies through runup inversions.

7. Conclusions

To explain the large and concentrated runup height of 7 m near Kaikoura following the 2016 tsunami, we propose a dual, submarine landslide-earthquake mechanism, rather than a previously-proposed offshore plate-interface rupture. Our dual tsunami source consists of the earthquake source of Hamling et al. (2017) and a theoretical landslide source located offshore Kaikoura. The main findings are:

1) Notwithstanding, the uncertainty over an offshore plate-interface rupture and its location, a submarine landslide offers a viable alternative. By numerical simulations of dual sources (the earthquake model of Hamling et al., 2017 and a submarine landslide), we successfully reproduced the near-field tsunami tide gauge record in Kaikoura as well as the observed runup height of 7 m.
2) Landslide dimensions and locations are: length = 10 km; width = 10 km; thickness = 150–175 m; and location: 173.7–174.3°E (longitude), 42.6–42.15°S (latitude). The volume of the landslide is 4.5–5.2 km^3. The landslide source is delayed 10–20 min compared to the earthquake origin time. The volume of the landslide agrees, to first order, with eroded sediment volumes calculated for landslides triggered by the earthquake, from before and after field surveys, where these are available.
3) Our dual source proposed here is consistent with tsunami waveforms and field runup data. Our dual model reproduces the seismic observations too, because the earthquake component of the dual source was validated with these data and the landslide component does not produce significant seismic signature on the seismic network. The novelty of our dual model over published source model is that it reproduces the field runup data whereas other source models fail.
4) This study highlights the importance of considering observed runup data for earthquake/tsunami source studies through runup inversions. While seismic/tsunami waveform inversions are commonly used for earthquake source studies, we showed that accurate source models can be achieved by both runup inversion and seismic/tsunami waveform inversions, especially if a landslide is involved.

Competing interests statement

The authors declare that they have no competing interests.

Acknowledgments

We used tide gauge records of GNS Science and Land Information New Zealand accessed through the IOC's website (http://www.ioc-

sealevelmonitoring.org/). Ian Hamling (GNS Science) shared his source model. Satoshi Kusumoto (University of Tokyo) helped with tsunami travel time analysis. We sincerely thank two anonymous reviewers for their constructive review comments which helped us to improve this article. This research was funded by Brunel Research Initiative and Enterprise Fund 2017/18 (BUL BRIEF) at the Brunel University London to the lead author (MH). DRT publishes with the approval of the CEO, British Geological Survey.

Appendix A. Supplementary data

Supplementary data to this article can be found online at https://doi.org/10.1016/j.oceaneng.2019.02.024.

References

Bai, Y., Lay, T., Cheung, K.F., Ye, L., 2017. Two regions of seafloor deformation generated the tsunami for the 13 November 2016, Kaikoura, New Zealand earthquake. Geophys. Res. Lett. 44 (13), 6597–6606.

Billi, A., Funiciello, R., Minelli, L., Faccenna, C., Neri, G., Orecchio, B., Presti, D., 2008. On the cause of the 1908 Messina tsunami, southern Italy. Geophys. Res. Lett. 35 (6). https://doi.org/10.1029/2008GL033251.

Duputel, Z., Rivera, L., 2017. Long-period analysis of the 2016 Kaikoura earthquake. Phys. Earth Planet. In. 265, 62–66.

Enet, F., Grilli, S.T., 2007. Experimental study of tsunami generation by three-dimensional rigid underwater landslides. J. Waterw. Port, Coast. Ocean Eng. 133, 442–454.

Fritz, H.M., Hager, W.H., Minor, H.E., 2004. Near field characteristics of landslide generated impulse waves. J. Waterw. Port, Coast. Ocean Eng. 130, 287–302.

Fritz, H.M., Kongko, W., Moore, A., McAdoo, B., Goff, J., Harbitz, C., Uslu, B., Kalligeris, N., Suteja, D., Kalsum, K., Titov, V., Gusman, A., Latief, H., Santoso, E., Sujoko, S., Djulkarnaen, D., Sunendar, H., Synolakis, C., 2007. Extreme runup from the 17 july 2006 Java tsunami. Geophys. Res. Lett. 34 (12), L12602. https://doi.org/10.1029/2007GL029404.

Fu, L., Heidarzadeh, M., Cukur, D., Chiocci, F.L., Ridente, D., Gross, F., Bialas, J., Krastel, S., 2017. Tsunamigenic potential of a newly discovered active fault zone in the outer Messina Strait, Southern Italy. Geophys. Res. Lett. 44 (5), 2427–2435.

Furlong, K.P., Herman, M., 2017. Reconciling the deformational dichotomy of the 2016 Mw 7.8 Kaikoura NZ earthquake. Geophys. Res. Lett. 44 (13), 6788–6791.

Geist, E.L., Lynett, P.J., Chaytor, J.D., 2009. Hydrodynamic modeling of tsunamis from the Currituck landslide. Mar. Geol. 264, 41–52.

Geoware, 2011. The Tsunami Travel Times (TTT). http://www.geoware-online.com/tsunami.html.

Glimsdal, S., Pedersen, G.K., Harbitz, C.B., Løvholt, F., 2013. Dispersion of tsunamis: does it really matter? Nat. Hazards Earth Syst. Sci. 13, 1507–1526.

Gusman, A.R., Murotani, S., Satake, K., Heidarzadeh, M., Gunawan, E., Watada, S., Schurr, B., 2015. Fault slip distribution of the 2014 Iquique, Chile, earthquake estimated from ocean-wide tsunami waveforms and GPS data. Geophys. Res. Lett. 42, 1053–1060.

Gusman, A.R., Satake, K., Gunawan, E., Hamling, I., Power, W., 2018. Contribution from multiple fault ruptures to tsunami generation during the 2016 Kaikoura earthquake. Pure Appl. Geophys. https://doi.org/10.1007/s00024-018-1949-z. https://link.springer.com/content/pdf/10.1007%2Fs00024-018-1949-z.pdf.

Hamling, I.J., Hreinsdóttir, S., Clark, K., Elliott, J., Liang, Fielding, E., Litchfield, N., Villamor, P., Wallace, L., Wright, T.J., et al., 2017. Complex multifault rupture during the 2016 Mw 7.8 Kaikōura earthquake, New Zealand. Science 356. https://doi.org/10.1126/science.aam7194.

Heidarzadeh, M., Satake, K., 2015a. Source properties of the 17 July 1998 Papua New Guinea tsunami based on tide gauge records. Geophys. J. Int. 202, 361–369.

Heidarzadeh, M., Satake, K., 2017a. A combined earthquake-landslide source model for the tsunami from the 27 november 1945 M 8.1 makran earthquake. Bull. Seismol. Soc. Am. 107, 1033–1040.

Heidarzadeh, M., Satake, K., 2017b. Possible dual earthquake-landslide source of the 13 November 2016 Kaikoura, New Zealand tsunami. Pure Appl. Geophys. 174 (10), 3737–3749.

Heidarzadeh, M., Pirooz, M.D., Zaker, N.H., Yalciner, A.C., 2009. Preliminary estimation of the tsunami hazards associated with the Makran subduction zone at the northwestern Indian Ocean. Nat. Hazards 48 (2), 229–243.

Heidarzadeh, M., Krastel, S., Yalciner, A.C., 2014. The state-of-the-art numerical tools for modeling landslide tsunamis: a short review. In: Submarine Mass Movements and Their Consequences, Chapter 43. Springer International publishing, pp. 483–495 ISBN: 978-3-319-00971-1.

Heidarzadeh, M., Murotani, S., Satake, K., Ishibe, T., Gusman, A.R., 2016a. Source model of the 16 September 2015 Illapel, Chile Mw 8.4 earthquake based on teleseismic and tsunami data. Geophys. Res. Lett. 43, 643–650.

Heidarzadeh, M., Harada, T., Satake, K., Ishibe, T., Gusman, A.R., 2016b. Comparative study of two tsunamigenic earthquakes in the Solomon Islands: 2015 Mw 7.0 normal-fault and 2013 Santa Cruz Mw 8.0 megathrust earthquakes. Geophys. Res. Lett. 43, 4340–4349.

Heidarzadeh, M., Murotani, S., Satake, K., Takagawa, T., Saito, T., 2017a. Fault size and depth extent of the Ecuador earthquake (Mw 7.8) of 16 April 2016 from teleseismic and tsunami data. Geophys. Res. Lett. 44, 2211–2219.

Heidarzadeh, M., Harada, T., Satake, K., Ishibe, T., Takagawa, T., 2017b. Tsunamis from strike-slip earthquakes in the Wharton Basin, northeast Indian Ocean: march 2016 Mw 7.8 event and its relationship with the April 2012 Mw 8.6 event. Geophys. J. Int. 211 (3), 1601–1612.

Hollinsworth, J., Ye, L., Avouac, J.P., 2017. Dynamically triggered slip on a splay fault in the Mw 7.8, 2016 Kaikoura (New Zealand) earthquake. Geophys. Res. Lett. 44 (8), 3517–3525.

Lane, E.M., Borrero, J., Whittaker, C.N., Bind, J., Chagué-Goff, C., Goff, J., Goring, D., Hoyle, J., Mueller, C., Power, W.L., Reid, C.M., Williams, J.H., Williams, S.P., 2017. Effects of inundation by the 14th november, 2016 Kaikōura tsunami on banks Peninsula, Canterbury, New Zealand. Pure Appl. Geophys. 174, 1855–1874.

Lay, T., Yue, H., Brodsky, E.E., An, C., 2014. The 1 April 2014 Iquique, Chile, Mw 8.1 earthquake rupture sequence. Geophys. Res. Lett. 41, 3818–3825.

Lewis, K.B., Barnes, P.M., 1999. Kaikoura Canyon, New Zealand: active conduit from near-shore sediment zones to trench-axis channel. Mar. Geol. 162, 39–69.

Massey, C., Townsend, D., Rathje, E., Allstadt, K.E., Lukovic, B., Kaneko, Y., Bradley, B., Wartman, J., Jibson, R.W., Petley, D.N., Horspool, N., 2018. Landslides triggered by the 14 november 2016 M w 7.8 Kaikōura earthquake, New Zealand. Bull. Seismol. Soc. Am. 108 (3B), 1630–1648.

Mathworks, 2017. MATLAB User Manual. The Math Works Inc., MA, USA, pp. 282.

Mountjoy, J.J., Howarth, J.D., Orpin, A.R., Barnes, P.M., Bowden, D.A., Rowden, A.A., Schimel, A.C.G., Holden, C., Horgan, H.J., Nodder, S.D., Patton, J.R., Lamarche, G., Gerstenberger, M., Micallef, A., Pallentin, A., Kane, T., 2018. Earthquakes drive large-scale submarine canyon development and sediment supply to deep-ocean basins. Science Advances 4 (3), eaar3748.

Okada, Y., 1985. Surface deformation due to shear and tensile faults in a half-space. Bull. Seismol. Soc. Am. 75, 1135–1154.

Okal, E.A., 1999. The 1998 Papua New Guinea tsunami: an overview. In: Proceedings of the Intl. Conf. Tsunamis, Paris, France, 26–28 May, pp. 111–116.

Okal, E.A., Synolakis, C.E., 2004. Source discriminants for near-field tsunamis. Geophys. J. Int. 158, 899–912.

Okal, E.A., Synolakis, C.E., Fryer, G.J., Heinrich, P., Borrero, J.C., Ruscher, C., Arcas, D., Guille, G., Rousseau, D., 2002. A field survey of the 1946 Aleutian tsunami in the far field. Seismol Res. Lett. 73, 490–503.

Okal, E.A., Plafker, G., Synolakis, C.E., Borrero, J.C., 2003. Near-field survey of the 1946 Aleutian tsunami on Unimak and Sanak islands. Bull. Seismol. Soc. Am. 93, 1226–1234.

Okal, E.A., Synolakis, C.E., Uslu, B., Kalligeris, N., Voukouvalas, E., 2009. The 1956 earthquake and tsunami in Amorgos, Greece. Geophys. J. Int. 178 (3), 1533–1554.

Power, W., Clark, K., King, D.N., Borrero, J., Howarth, J., Lane, E.M., Goring, D., Goff, J., Chagué-Goff, C., Williams, et al., 2017. Tsunami runup and tide-gauge observations from the 14 November 2016 M7.8 Kaikōura earthquake, New Zealand. Pure Appl. Geophys. 174 (7), 2457–2473.

Rabinovich, A.B., 1997. Spectral analysis of tsunami waves: Separation of source and topography effects. J. Geophys. Res. 102, 12663–12676.

Ren, Z.Y., Zhao, X., Liu, H., 2015. Dispersion effects on tsunami propagation in the South China Sea. J. Earthq. Tsunami. 9 (5), 1540001.

Satake, K., 1995. Linear and nonlinear computations of the 1992 Nicaragua earthquake tsunami. Pure Appl. Geophys. 144, 455–470.

Satake, K., Tanioka, Y., 2003. The July 1998 Papua New Guinea earthquake: mechanism and quantification of unusual tsunami generation. Pure Appl. Geophys. 160, 2087–2118.

Satake, K., Fujii, Y., Harada, T., Namegaya, Y., 2013. Time and space distribution of coseismic slip of the 2011 Tohoku earthquake as inferred from tsunami waveform data. Bull. Seismol. Soc. Am. 103, 1473–1492.

Synolakis, C., Kânoğlu, U., 2015. The Fukushima accident was preventable. Phil. Trans. R. Soc. A 373. https://doi.org/10.1098/rsta.2014.0379.

Synolakis, C.E., Bardet, J.P., Borrero, J.C., Davies, H.L., Okal, E.A., Silver, E.A., Sweet, S., Tappin, D.R., 2002. The slump origin of the 1998 Papua New Guinea tsunami. Proc. Roy. Soc. Lond. A 458 (2020), 763–789.

Tappin, D.R., Watts, P., McMurtry, G.M., Lafoy, Y., Matsumoto, T., 2001. The Sissano, Papua New Guinea tsunami of July 1998- offshore evidence on the source mechanism. Mar. Geol. 175, 1–23.

Tappin, D.R., Watts, P., Grilli, S.T., 2008. The Papua New Guinea tsunami of 17 July 1998: anatomy of a catastrophic event. Nat. Hazards Earth Syst. Sci. 8, 243–266.

Tappin, D.R., Grilli, S.T., Harris, J.C., Geller, R.J., Masterlark, T., Kirby, J.T., Shi, F., Ma, G., Thingbaijam, K.K.S., Mai, P.M., 2014. Did a submarine landslide contribute to the 2011 Tohoku tsunami? Mar. Geol. 357, 344–361.

Tinti, S., Armigliato, A., Manucci, A., Pagnoni, G., Zaniboni, F., Yalciner, A.C., Altinok, Y., 2006. The generating mechanisms of the August 17, 1999 Izmit Bay (Turkey) tsunami: regional (tectonic) and local (mass instabilities) causes. Mar. Geol. 225, 311–330.

Walters, R.A., Barnes, P., Lewis, K., Goff, J.R., 2006. Locally generated tsunami along the Kaikoura coastal margin: Part 2. Submarine landslides. N. Z. J. Mar. Freshw. Res. 40, 17–28.

Watts, P., Grilli, S.T., Kirby, J.T., Fryer, G.J., Tappin, D.R., 2003. Landslide tsunami case studies using a Boussinesq model and a fully nonlinear tsunami generation model. Nat. Hazards Earth Syst. Sci. 3, 391–402.

Watts, P., Grilli, S.T., Tappin, D.R., Fryer, G.J., 2005. Tsunami generation by submarine mass failure. II: predictive equations and case studies. J. Waterw. Port, Coast. Ocean Eng. 131, 298–310.

Weatherall, P., Marks, K.M., Jakobsson, M., Schmitt, T., Tani, S., Arndt, J.E., Rovere, M., Chayes, D., Ferrini, V., Wigley, R., 2015. A new digital bathymetric model of the world's oceans. Earth Space Science 2, 331–345. https://doi.org/10.1002/2015EA000107.